The Astrophysical Journal, 617:232–239, 2004 December 10

O VII AND O VIII ABSORPTION BY HOT GAS IN THE VICINITY OF THE GALAXY

Barry McKernan,[1] Tahir Yaqoob,[2,3] and Christopher S. Reynolds[1]

Received 2004 June 26; accepted 2004 August 26

ABSTRACT

We searched for evidence of soft X-ray absorption by hot gas in the vicinity of the Galaxy in a small sample of 15 type I active galactic nuclei (AGNs) observed with the high resolution X-ray gratings on board *Chandra*. We find that around half of the sight lines in our sample exhibit absorption due to local H- or He-like oxygen (or both) at confidence levels ranging from >90% to >3 σ. Depending on the sight line, the absorption can be identified with hot gas in particular local structures, the Local Group (LG), or the putative local hot intergalactic medium (IGM). Several sight lines in our sample coincide with sight lines in a study of O VI absorption by local gas, so an assumption of collisional ionization equilibrium (CIE) allows us to constrain the temperature of the local hot gas. In the southern Galactic hemisphere, we identify absorption along the sight line to Fairall 9 with the Magellanic Stream, and this gas has $10^{5.75} < T < 10^{6.35}$ K if CIE applies. There may be a blend of O VII absorption features along the sight line toward Mrk 509. LG clouds along this sight line may interact with a hot Galactic corona or a low-density LG medium (or the IGM). The sight line to 3C 120 does not appear to be associated with either local structure or UV-absorbing gas and may correspond to the local hot IGM. Gas in the Magellanic Stream extension along the sight line to Ark 564 has $T < 10^{6.1}$ K if it is in CIE. We show that hot absorbing outflows apparently detected in the spectra of NGC 4051, PDS 456, and PG 1211+143 could actually correspond to absorption by hot, local gas since the outflow velocity from each of these AGNs coincides with the respective cosmological recession velocity of the AGN. Our work implies that apparent mildly relativistic outflows from some QSOs are more likely to correspond to signatures of local, hot gas.

Subject headings: galaxies: active — galaxies: ISM — galaxies: Seyfert — techniques: spectroscopic — X-rays: ISM

1. INTRODUCTION

One of the most important new results from the *Chandra* and *XMM-Newton* X-ray satellites has been the discovery of hot, highly ionized gas in the vicinity of our Galaxy (at $z = 0$) and possibly beyond (at $z > 0$). Simulations indicate that around half of the baryonic matter at low redshift in a cold dark matter universe is expected to live in filaments, shock-heated to $\sim 10^5$–10^7 K, that surround galaxies and clusters of galaxies (see, e.g., Cen & Ostriker 1999; Davé et al. 2001, and references therein). The "warm" ($\sim 10^5$–10^6 K) component of this warm–hot intergalactic medium (WHIGM) has been observed in absorption in the UV band (e.g., Tripp et al. 2000; Sembach et al. 2003, and references therein). However, much (possibly most) of the WHIGM is expected to be hotter than this, so the high spectral resolution X-ray detectors such as those aboard *Chandra* and *XMM-Newton* are best placed for investigating the "hot" component of the missing baryons.

X-ray absorption due to local ($z = 0$) hot gas has been discovered recently (Nicastro et al. 2002; Fang et al. 2002, 2003; Cagnoni 2002; Rasmussen et al. 2003; McKernan et al. 2003a, 2003b). The clearest X-ray spectral signature of hot gas in the vicinity of our Galaxy consists of O VII and O VIII absorption features imprinted in spectra of X-ray–bright active galactic nuclei (AGNs) at $z = 0$ in the observed frame (Hellsten et al. 1998; Perna & Loeb 1998). Of course, such absorption features need not be associated with missing baryons embedded the in Local Group WHIGM. O VII and O VIII absorption at $z = 0$ could also result from absorption by highly ionized gas in such local Galactic morphological structures as the Magellanic Stream (MS), a complex of high-velocity gas tidally torn from the Magellanic Clouds as they interact with the Milky Way. Hot gas associated with local structures and with an extended Galactic halo, as well as Local Group WHIGM, has been observed in the UV-band (with *FUSE*) along 59 sight lines toward AGNs (Sembach et al. 2003, hereafter S03). Even if there are no known local structures along the sight line to a particular AGN, there may still be some ambiguity over the location of the absorbing gas. Around half of all type I AGNs exhibit strong absorption due to a partially ionized, optically thin, circumnuclear material known as the "warm absorber" (see, e.g., Reynolds 1997; George et al. 1998, and references therein). Observations with *Chandra* and *XMM-Newton* have confirmed that the warm absorbing material is outflowing with typical velocities of hundreds of km s^{-1}. Therefore, if the AGN is at very low redshift ($cz \sim$ few hundred km s^{-1}), absorption that is actually local to our Galaxy at $z \sim 0$ could be misinterpreted as absorption due to outflowing gas in the AGN.

The spectral signature of "hot" WHIGM in absorption at $z > 0$ is also ambiguous. Absorption signatures of WHIGM outside the Local Group (at $z > 0$) have been claimed along the sight lines toward several X-ray–bright AGNs, including PKS 2155−304 (Nicastro et al. 2002; Fang et al. 2002), 3C 273 (Fang et al. 2003), Mrk 421 (Cagnoni 2002; Rasmussen et al. 2003), and 3C 120 (McKernan et al. 2003b). However, as pointed out by Fang et al. (2002) and McKernan et al. (2003b), all of these sources possess relativistic outflows at a small

[1] Department of Astronomy, University of Maryland, College Park, MD 20742.
[2] Department of Physics and Astronomy, The Johns Hopkins University, 3400 North Charles Street, Baltimore, MD 21218.
[3] Laboratory for High Energy Astrophysics, NASA Goddard Space Flight Center, Greenbelt, MD 20771.

TABLE 1
THE *Chandra* HETGS SAMPLE OF TYPE I AGNS

Source (1)	Galactic longitude (deg) (2)	Galactic latitude (deg) (3)	Redshift (z) (4)	Galactic $N_{\rm H}$ (10^{20} cm^{-2})[a] (5)	Exposure (ks) (6)
Fairall 9	295.07	−57.83	0.04600	3.0	80
3C 120[b]	190.37	−27.40	0.03301	12.30	58
NGC 3227	216.99	55.45	0.00386	2.15	47
NGC 3516	133.24	44.40	0.00884	3.05	200
NGC 3783	287.46	22.95	0.00973	8.50	850
NGC 4051	148.88	70.09	0.00242	1.31	80
Mrk 766	190.68	82.27	0.01293	1.80	90
NGC 4593	297.48	57.40	0.00831	1.97	79
MCG−6-30-15	313.29	27.68	0.00775	4.06	126
IC 4329A	317.50	30.92	0.01605	4.55	60
Mrk 279	115.04	46.86	0.03045	1.64	116
NGC 5548	31.96	70.50	0.01717	1.70	82
Mrk 509	35.97	−29.86	0.03440	4.44	60
NGC 7314	27.14	−59.74	0.00474	1.46	97
Ark 564	92.14	−25.34	0.02467	6.40	50

NOTE.—Cols. (2) and (3): Galactic coordinates of the source (from NED). Col. (4): Redshift of the source (from NED). Redshift was deduced from observations of the 21 cm H I line where possible, since optical estimates of z may be confused by AGN outflow.

[a] Galactic column density from Elvis et al. (1989), except for Mrk 509 (Murphy et al. 1996). The Galactic column density toward F9, NGC 3227, NGC 3516, NGC 3783, NGC 5548, Mrk 766, NGC 7314, and Ark 564 was estimated from interpolations from the measurements of Stark et al. (1992).

[b] 3C 120 is also classified as a broad-line radio galaxy (NED).

angle to the sight lines. An AGN at $z_{\rm AGN}$ possessing such an outflow could imprint blueshifted absorption features at several thousand km s^{-1}, thereby mimicking the effect of absorption at $0 < z_{\rm IGM} < z_{\rm AGN}$. One way of resolving this ambiguity is to investigate absorption features in a sample of AGNs that *do not* possess such relativistic outflows, and we study such a sample in the present paper.

In this paper, we investigate a sample of AGNs observed with the High Energy Transmission Grating Spectrometer (HETGS; Markert et al. 1994) on board *Chandra*. The uniform analysis of the data from these AGNs and the results of the analysis, in particular the characterization of the AGN continua and the warm absorption in AGNs, have been discussed in detail by McKernan et al. (2004). Here we search the AGN sample of McKernan et al. (2004) for absorption due to highly ionized gas in the vicinity of the Galaxy ($z = 0$).

2. THE SAMPLE AND DATA ANALYSIS

Table 1 lists the AGN sample assembled by McKernan et al. (2004) observed using the HETGS (Markert et al. 1994) on board *Chandra*. Also listed in Table 1 are the AGN Galactic latitude and longitude (from NED[4]), the AGN redshift (also from NED, using 21 cm H I radiation measurements where possible), the Galactic column density, and the total exposure of the spectra. The sample, including selection criteria, is discussed in detail in McKernan et al. (2004). The *Chandra* HETGS consists of two grating assemblies, a high-energy grating (HEG) and a medium-energy grating (MEG). We used the MEG as our primary instrument since the effective area of the HEG falls off sharply below 0.8 keV. The MEG has a FWHM spectral resolution of $\sim$280 km s^{-1} at $\sim$0.5 keV. We used only the combined ± 1 orders of the MEG data in our analysis. The *Chandra* data were reprocessed and analyzed according to the methods outlined in McKernan et al. (2004). Note that 5 of the 15 AGNs were also observed with *Chandra* low-energy transmission gratings (LETGS). The high-resolution camera (HRC) was used in four of these observations. However, order separation is not possible with the HRC. This fact, plus our aim to study the spectra at the highest spectral resolution, means that we did not use the *Chandra* LETGS observations of the AGNs in our sample (the LETGS has a spectral resolution of only 0.05 Å FWHM).

Since there has been a systematic search for O VI absorption by hot gas in the vicinity of the Galaxy along the sight lines to AGNs by S03, and since oxygen is the most abundant element that is detectable in the soft X-ray band, we searched the *Chandra* spectra for evidence of the strongest absorption transitions in oxygen, namely O VII (r) $1s$–$2p$ and O VIII Lyα (which have oscillator strengths of $f = 0.415$ and 0.696, respectively) in the velocity range $cz = 0 \pm 1200$ km s^{-1} in the local standard of rest (LSR). Once we measured the oxygen absorption profiles, we used the extrapolated linear approximation to the curves of growth[5] to obtain a lower limit on the ionic column density ($N_{\rm ion}$), if a *lower limit* on the equivalent widths (EW) of the absorption feature was available. Such a lower limit on $N_{\rm ion}$ is valid for any value of the velocity width (b) of the absorber. Where no lower limit on the EW exists, absorption is not significant (at 90% confidence). However, in this case, for an assumed b-value, we can use the *upper limit* on the EW (if it exists) to get an upper limit on $N_{\rm ion}$. In such cases, we assumed a velocity width of $b \sim 100$ km s^{-1}, since this is about the smallest width of a feature that the MEG can resolve, although it is considerably larger than the average value of $\langle b \rangle = 40 \pm 13$ km s^{-1} found by S03 in the local hot gas along 59 sight lines. S03 indicate that the O VI along most sight lines

[4] See http://nedwww.ipac.caltech.edu/forms/byname.html.

[5] The linear part of the curves of growth implies that $N_{\rm ion} = 1.13 \times 10^{17} (\mathrm{EW}/f\lambda^2)$, where $N_{\rm ion}$ is the ionic column density (cm^{-2}), EW is the equivalent width of the absorption feature (in mÅ), f is the oscillator strength of the transition, and λ is in Å.

TABLE 2
Spectral Fitting Results for Hot Gas at $z = 0$

Source (1)	EW (O VII (r)) (eV) [ΔC] (2)	EW (O VIII Lyα) (eV) [ΔC] (3)	$N_{\rm O\ VII}$ ($\rm cm^{-2}$) (4)	$N_{\rm O\ VIII}$ ($\rm cm^{-2}$) (5)	Velocity ($\rm km\ s^{-1}$) (6)	$N_{\rm O\ VI}$[a] ($\rm cm^{-2}$) (7)	Velocity[a] ($\rm km\ s^{-1}$) (8)	ID[a,b] (9)
F9	$0.79^{+\ldots}_{-0.29}$[c] [7.7]	<0.67 [0.5]	>16.10	<16.60	-180 ± 155	14.33 ± 0.14	185^{+90}_{-85}	MS
3C 120	$0.60^{+\ldots}_{-0.57}$[c] [3.0]	$0.94^{+\ldots}_{-0.57}$[c] [5.3]	>14.85	>15.73	120 ± 105	...	...	...
NGC 3783	$0.61^{+0.27}_{-0.25}$ [16.8]	<0.36 [1.4]	<16.65, >15.85	<15.88	190^{+105}_{-155}	...	...	[EPn]
NGC 4051	$1.63^{+\ldots}_{-0.65}$[c] [16.8]	$0.85^{+0.28}_{-0.32}$ [12.1]	>16.45	<18.38, >15.85	110 ± 115	...	...	[EPn]
NGC 4593	<0.74 [5.5]	<0.70 [2.3]	<17.25	<16.75	85^{+175}_{-105}	...	...	[EPn]
NGC 5548	$0.69^{+\ldots}_{-0.44}$[c] [5.0]	$1.06^{+\ldots}_{-0.48}$[c] [9.8]	>15.74	>15.93	-70 ± 165	<13.84[d]	...	...
Mrk 509	<0.57 [6.7]	$0.58^{+0.28}_{-0.43}$ [4.3]	<16.75	<16.13,[c] >15.28	100 ± 155	14.24 ± 0.10	247^{+67}_{-98}	LG
	...	...	...	...	...	13.76 ± 0.19	-143^{+43}_{-37}	LG
	...	...	...	...	...	13.55 ± 0.28	152^{+48}_{-37}	LG

Note.—Inverted Gaussians with redshift fixed at $z = 0$ were added to the continuum at the rest-frame energies of O VII (r) and O VIII Lyα. The Gaussian model component energies were free to vary up to ± 1200 km $\rm s^{-1}$ from $z = 0$. The continuum model for each AGN was the best-fit power law or broken power law from McKernan et al. 2004. Cols. (2) and (3): Best-fit EW for O VII (r) and O VIII Lyα, respectively, and (in brackets) the improvement in the fit statistic upon the addition of the inverted Gaussian model component to the continuum. Cols. (4) and (5): Ionic column densities of O VII and O VIII, respectively, as estimated from a curve-of-growth analysis described in the text. Lower limit on ionic column densities are valid for all values of b. Upper limits are valid for an assumed velocity width of 100 km $\rm s^{-1}$ (unless specified otherwise), which is approximately the lower bound on the instrumental resolution. A choice of $b = 100$ km $\rm s^{-1}$ is larger than the values inferred by S03 for local O VI absorption features. Col. (6): Weighted mean velocity centroid offset from $z = 0$ (LSR) of the two absorption features, except for F9, NGC 3783, NGC 4593, and Mrk 509, where this is the offset velocity of the strongest absorption feature. Col. (7): O VI column density (where available) along the line of sight to the AGN as determined by *FUSE* (S03). Col. (8): Velocity of the $z = 0$ O VI absorber components (where available). Velocities are rounded to the nearest 5 km $\rm s^{-1}$, and a negative value denotes blueshift from $z = 0$ (in the LSR). Col. (9): Local structure identified by S03 with the O VI absorption along the sight lines to the AGNs (IDs in brackets are those proposed by us).

[a] From S03.
[b] LG = Local Group, MS = Magellanic Stream, EPn = Extreme Positive north.
[c] No meaningful upper limits because of poor statistics and possible line saturation.
[d] At 3 σ confidence level.
[e] Valid for all values of b.

is collisionally ionized. This suggests that unresolved saturated structure is unlikely in the absorption features. We tested the possibility of unresolved saturated structure in the absorption features (and thereby double-checked the estimates of ionic column density) by deducing the threshold depths of the bound-free O VII and O VIII absorption edges (0.7393 keV and 0.8714 keV in the rest frame, respectively).

3. SPECTRAL FITTING

We used XSPEC version 11.2.0 for spectral fitting to the MEG spectra. All spectral fitting was carried out based on the best-fit continuum models from McKernan et al. (2004). Spectral fitting was carried out in the 0.5–5 keV energy band, excluding the 2.0–2.5 keV region, which suffers from systematics as large as ~20% in the effective area because of limitations in the calibration of the X-ray telescope.[6] We analyzed data binned at ~0.02 Å, which is approximately the MEG FWHM spectral resolution (0.023 Å). MEG spectral resolution corresponds to FWHM velocities of ~280 and 560 km $\rm s^{-1}$ at observed energies of 0.5 and 1.0 keV, respectively. We used the C-statistic (Cash 1976) for finding best-fit model parameters and quote 90% confidence, one-parameter errors.

We proceeded to fit the MEG spectra for the oxygen absorption transitions by adding an inverted Gaussian model component to the best-fit continuum models detailed in McKernan et al. (2004). We fixed the redshift of the Gaussian components at $z = 0$ and allowed the rest energy of the component to vary by ± 1200 km $\rm s^{-1}$ from the rest-frame energies of O VII (r) (0.5740 keV) and O VIII Lyα (0.6536 keV) The allowed velocity range is identical to that used by S03 in their search for O VI absorption in the vicinity of the Milky Way. In fitting the bound-free absorption edges, we fixed the edge energies at the rest-frame values (0.7393 and 0.8714 keV for O VII and O VIII, respectively), and we fixed the redshift at $z = 0$.

[6] See http://asc.harvard.edu/cal.

4. RESULTS

Of the 15 AGNs in our sample, we find that seven AGNs exhibit an improvement in the fit statistic at >90% confidence ($\Delta C \geq 6.3$ for three additional parameters) when we fit the spectra with inverted Gaussian model components corresponding to highly ionized oxygen absorption features (O VII (r) or O VIII Lyα, or both) at $z = 0$. Table 2 shows the spectral fitting results for these seven AGNs, including the EW of the absorption features, the velocity offset from LSR of the Gaussian centroid, and limits on the column densities of highly ionized oxygen as estimated from a curve-of-growth analysis outlined in § 2. Also listed in Table 2 are the column density and offset velocity from LSR of O VI along the sight lines (from S03) where available. Column (9) of Table 2 lists the local structure associated by S03 with the sight lines to each AGN (where available). We could not obtain meaningful upper limits from Gaussian fits to the EW of 6 of the 16 absorption features listed in Table 2. This is most likely due to poor statistics, but it could also indicate line saturation.

O VII (r) absorption due to local hot gas is present in the spectra of NGC 3783 and NGC 4051 at >3 σ significance ($\Delta C \geq 14.2$ for three additional parameters) and in the spectra of Fairall 9 (F9) and Mrk 509 at >90% confidence ($\Delta C \geq 6.3$ for three additional parameters). O VIII absorption due to local gas is present only in the spectra of NGC 5548 and NGC 4051 at >90% confidence. Although both of the absorption signatures toward 3C 120 and NGC 4593 are detected at <90% confidence, we include these results in Table 2 because the detection of *both* local absorption signatures corresponds to a confidence level >90%. Of the 15 AGNs spectra in our sample only one

TABLE 3
RESULTS FROM FITS TO OXYGEN ABSORPTION EDGES AT $z = 0$

Source (1)	$N_{\rm O\ VII}$ ($\rm cm^{-2}$) (2)	$N_{\rm O\ VIII}$ ($\rm cm^{-2}$) (3)
F9	<17.22	<17.46
3C 120	<17.34	$17.87^{+0.20}_{-0.23}$
NGC 3783	<16.09	$17.21^{+0.27}_{-0.90}$
NGC 4051	$17.56^{+0.18}_{-0.30}$	<17.70
NGC 4593	$17.17^{+0.29}_{-1.25}$	<17.54
NGC 5548	<17.27	<17.55
Mrk 509	<17.23	<17.51

NOTE.—Cols. (2) and (3): Column densities of O VII and O VIII, respectively, as estimated from depths of the corresponding bound-free edges (rest-frame edge threshold energies are 0.7398 and 0.8714 keV for O VII and O VIII, respectively). The absorption cross sections at the bound-free edge threshold energies are 2.42×10^{-19} and 0.99×10^{-19} $\rm cm^2$ for O VII and O VIII, respectively (Verner et al. 1996). The limit on $N_{\rm O\ VIII}$ in NGC 3783 does not agree with the results from Table 2. However, NGC 3783 has a very complicated continuum due to strong absorption intrinsic to the AGN (see, e.g., McKernan et al. 2004 for details).

(NGC 4051) exhibits absorption due to *both* local O VII (r) *and* local O VIII Lyα—at >3 σ and >99% confidence ($\Delta C \geq 14.2$ and ≥ 11.3 for three additional parameters, respectively).

Table 3 shows the results from fitting O VII and O VIII absorption edges at $z = 0$ to the spectra of AGNs in Table 2. In general, the absorption edge fits in Table 3 provide upper limits to the O VII and O VIII column densities of the hot, local gas and agree with the limits on $N_{\rm O\ VII}$ and $N_{\rm O\ VIII}$ from Table 2. The exception is the limit on $N_{\rm O\ VIII}$ in NGC 3783, which does not agree with Table 2. However, NGC 3783 has a very complicated continuum due to strong absorption intrinsic to the AGN (see, e.g., McKernan et al. 2004 for details).

Figure 1 is a multipanel plot showing velocity profiles from the AGNs in Table 2. The profiles are centered on the O VII (r) transition energy in the LSR (0.5740 keV) and the O VIII Lyα transition energy (0.6536 keV; both energies are denoted by vertical dashed lines). Superposed is the best-fit inverted Gaussian absorption line model (from Table 2) and continuum (*solid line*). The vertical dashed line in Figures 1*d*–1*k* at +725 km $\rm s^{-1}$ denotes the redshift velocity (cz) of NGC 4051. Note that absorption toward this AGN could correspond either to absorption by gas in the vicinity of our Galaxy or to intrinsic absorption in the AGN at an outflow velocity of 615 ± 115 km $\rm s^{-1}$ (see discussion in § 6). There is a hint of additional absorption at ~ -400 km $\rm s^{-1}$ toward Mrk 509 (Figs. 1*g*–1*n*). According to S03 there are three UV absorption components due to Local Group (LG) gas along this sight line spanning $\sim$550 km $\rm s^{-1}$ in offset velocity. Therefore, we might expect broad absorption profiles from a blend of several narrow components along the sight line to Mrk 509. In fact, a considerably broader and deeper O VII (r) profile can be fit to the Mrk 509 data, but the required width of the resulting feature is greater than the width of the velocity range that we are studying here (2400 km $\rm s^{-1}$). Collins et al. (2004) suggest that broad, high-velocity O VI absorption along this sight line arises from shock ionization at bow shock interfaces produced from infalling high-velocity clouds (HVCs).

Eight AGNs from the 15 listed in Table 1 did not exhibit an improvement in the fit statistic when their spectra were fit with O VII (r) and O VIII Lyα absorption features. The spectra of three of these eight AGNs, namely NGC 3227, NGC 3516, and NGC 7314, were so strongly absorbed at energies $\leq$0.7 keV that it was not possible to obtain limits on the column densities of $N_{\rm O\ VII}$ and $N_{\rm O\ VIII}$ along these sight lines. Table 4 lists the upper limits of $N_{\rm O\ VII}$ and $N_{\rm O\ VIII}$ along the sight lines to the remaining five AGNs. Of these five AGNs, only Ark 564 has a sight line that coincides with the S03 study and exhibits O VI absorption associated by S03 with the local MS extension.

5. COMPARISON WITH O VI ABSORPTION RESULTS

S03 searched for O VI (λ1031.926) absorption along 102 sight lines at high Galactic latitudes of $|b| \geq 30^\circ$ toward UV-bright AGNs. Some 59 of the 102 sight lines revealed a total of 84 high-velocity ($|v| > 100$ km $\rm s^{-1}$ in the LSR) O VI absorption components at ≥ 3 σ confidence level. Three of these 59 sight lines coincide with sight lines in our sample (see Table 2). The sight lines to the 15 AGNs in our sample, plus six AGNs in the literature toward which WHIGM at $z = 0$ has been detected or searched for, are shown in a Hammer-Aitoff projection in Figure 2. Plus signs indicate a lack of highly ionized local gas (at 90% confidence). Open diamonds indicate detections (at >90% confidence) of highly ionized local gas with no corresponding *FUSE* sight lines. Filled circles indicate sight lines along which highly ionized oxygen has been detected (at >90% confidence) with corresponding *FUSE* observations of O VI absorption. It is useful to compare this plot with similar projections in S03 (see, e.g., their Fig. 6). While the number of points in Figure 2 is small, we can begin to associate very highly ionized absorption along some of these sight lines with the hot structures discussed by S03.

The average value of the O VI column density ($N_{\rm O\ VI}$) detected by S03 was $\langle \log N_{\rm O\ VI} \rangle = 13.95 \pm 0.34$, which is considerably lower than the average column of $\langle \log N_{\rm O\ VI} \rangle = 14.38 \pm 0.18$ in the Galactic thick disk and halo. By comparison, along the sight lines in our sample, $\langle \log N_{\rm O\ VII} \rangle$ and $\langle \log N_{\rm O\ VIII} \rangle$ seem to lie in the range $\sim$16–17 (see Table 2). The highest values of $N_{\rm O\ VI}$ found by S03 are associated by them with known local structures such as the MS, Complex C, and Extreme Positive north (EPn). The highest values of $N_{\rm O\ VII}$ and $N_{\rm O\ VIII}$ from our Table 2 may also be associated with local structure (EPn and MS).

O VI in low-redshift IGM is far more likely to be collisionally ionized than photoionized (Heckman et al. 2002; S03). Therefore, if we assume that the hot gas in the vicinity of the Galaxy is in collisional ionization equilibrium (CIE), and that the O VI and O VIII absorption occurs in the same gas, we can establish temperature constraints on the gas. Sutherland & Dopita (1993) calculate $N_{\rm O\ VII}/N_{\rm O\ VI}$ and $N_{\rm O\ VIII}/N_{\rm O\ VI}$ for gas in CIE, and we can use these values to constrain the temperature of the local gas toward several of the AGNs in our sample. In the case of the F9 sight line, CIE implies $10^{5.75} < T < 10^{6.35}$ K. For the gas along the sight line to Mrk 509, CIE implies $T < 10^{6.20}$ K, although Collins et al. (2004) suggest that nonequilibrium ionization occurs along this sight line, in which case CIE is ruled out. Likewise, if the hot gas along the sight line to NGC 5548 and Ark 564 is in CIE, then $T > 10^{5.80}$ K and $T < 10^{6.10}$ K for the NGC 5548 and Ark 564 sight lines, respectively.

S03 find that O VI absorption features at $z = 0$ have a mean centroid velocity relative to LSR of -33 ± 207 km $\rm s^{-1}$. The mean centroid velocity of the features listed in Table 2 is 70 ± 25 km $\rm s^{-1}$. S03 found that the centroids of the O VI features are generally significantly redshifted at Galactic longitudes $180^\circ < l < 360^\circ$ and significantly blueshifted at Galactic longitudes $0^\circ < l < 180^\circ$. The limited size of our sample and the limited velocity resolution of *Chandra* (MEG has a FWHM resolution of $\sim$280 km $\rm s^{-1}$ at energies around O VII (r)) mean that we cannot establish a similar pattern in our data. S03

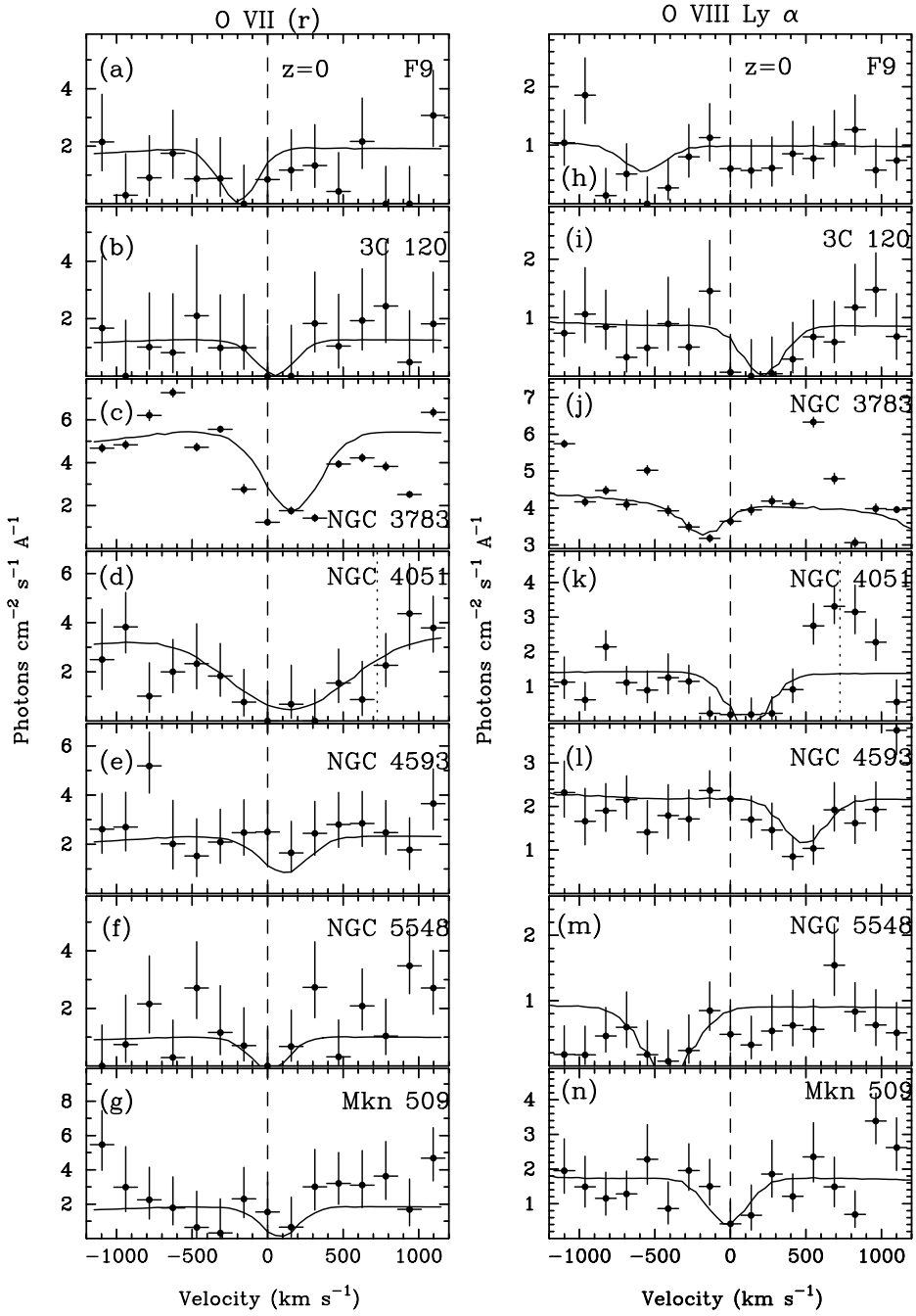

FIG. 1.—Velocity profiles from combined ±1 order *Chandra* MEG data from the AGNs in Table 2, centered on the LSR O VII (*r*) transition energy (0.57396 keV) in the left column panels and on the O VIII Lyα transition energy (0.65362 keV) in the right column panels. A positive velocity indicates a redshift relative to these energies. The velocity spectra data have been uniformly binned at 0.3 eV, which is approximately the limit of the MEG resolution. Vertical dashed lines at 0 km s^{-1} correspond to the location of the O VII (*r*) transition energy (*left panels*) or the O VIII Lyα transition energy (*right panels*) in the LSR. Vertical dotted lines in panels (*d*) and (*k*) indicate the rest frame of NGC 4051. The remaining AGN rest energies lie outside the ±1200 km s^{-1} range of these panels. Note that in NGC 4051, the broad absorption features indicate that there may be a blend of intrinsic warm absorption in the AGN (outflowing at ~600 km s^{-1}) and local absorption. Superposed is the best-fit inverted Gaussian absorption line model (from Table 2) and continuum (*solid line*). The models are calculated from the best-fit Gaussian model in Table 2 since most of the results in Table 2 are independent of the value of b ($=\sqrt{2}\sigma$).

also found that the average high velocity feature width is $\langle b \rangle = 40 \pm 13$ km s^{-1}. By comparison, we have *assumed* a turbulent velocity of $b \sim 100$ km s^{-1} where necessary to establish limits on ionic column density. Around half the features shown in Figure 1 and listed in Table 2 may be saturated, suggesting that the actual turbulent velocity of the gas may be <100 km s^{-1}; however, we are limited by the MEG velocity resolution and (generally) the low signal-to-noise ratio of the data in this energy range.

The LG features discussed by S03 include the LG itself and EPn. The average offset velocity of the centroid of the absorption features that S03 identify with the Local Group itself is -55 ± 212 km s^{-1} in the LSR. LG features have *no* obvious corresponding H I 21 cm emission at similar velocities directly along the sight lines. All of the LG clouds are located in the southern Galactic hemisphere, mostly in the $35^\circ < l < 140^\circ$ Galactic longitude range (similar to the range in Galactic longitude of the MS extension absorption features). Four of the

TABLE 4

NULL RESULTS FOR HOT GAS AT $z = 0$

Source	$N_{\rm O\ VII}$ ($\rm cm^{-2}$)	$N_{\rm O\ VIII}$ ($\rm cm^{-2}$)
Mrk 766	<17.85	<16.28
MCG −6-30-15	<16.90	<16.18
IC 4329A	<17.85	<16.13
Mrk 279	<17.65	<18.58
Ark 564	<16.10	<15.58

NOTE.—Same as for Table 2. The spectra of NGC 3227, NGC 3516, and NGC 7314 were too strongly absorbed at <0.7 keV to obtain limits on $N_{\rm O\ VII}$ and $N_{\rm O\ VIII}$.

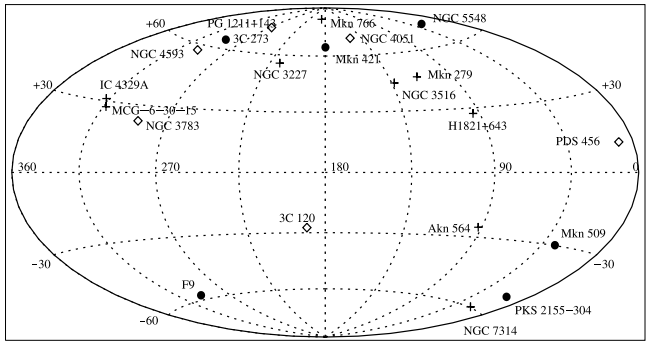

FIG. 2.—All-sky Hammer-Aitoff projection of the sight lines to the 15 AGNs in this study, plus sight lines for six additional AGNs in the literature. The additional AGNs are Mrk 421 (Cagnoni 2002; Rasmussen et al. 2003), PKS 2155−304 (Nicastro et al. 2002), 3C 273 (Fang et al. 2003), PG 1211+143 (Pounds et al. 2003), PDS 456 (Reeves et al. 2003), and H1821+643 (Mathur et al. 2003). In this projection, the Galactic anticenter is at the center of the figure, and Galactic longitude increases to the left. *Plus signs*: Nondetection of local, hot gas. *Open diamonds*: Detection of local, hot gas along the sight lines at >90% confidence but with no corresponding *FUSE* observations. *Filled circles*: Detections of local, hot gas along the sight lines *and* corresponding *FUSE* observations of O VI. PG 1211+143 and PDS 456 are included because the apparent intrinsic absorption in their spectra has an outflow velocity that coincides with our LSR.

seven sight lines listed in Table 2, namely NGC 3783, NGC 4051, NGC 4593 (all EPn), and Mrk 509 (LG) can likewise be identified with the Local Group.

The sight line to Mrk 509 passes through two high-velocity clouds (HVCs) detected in absorption in C IV with velocity centroids at -283 and -228 km $\rm s^{-1}$. The HVCs have ionization properties consistent with clouds irradiated by local extragalactic background radiation according to Sembach et al. (1999); however, the amount of O VI inferred along the sight line suggests that this is not the only source of ionization. S03 and Collins et al. (2004) suggest that these clouds interact with a hot Galactic corona or a low-density LG medium (the $z = 0$ WHIGM). As noted above, the O VII (r) feature in Figure 1*f* can be fitted with a broader inverted Gaussian profile than in Table 2, since the line shape is poorly constrained. The O VIII feature along this sight lines appears much weaker, however, which suggests an upper limit to the temperature of the local gas along this sight line.

In the southern Galactic hemisphere, the sight line to F9 passes through the MS, and the sight line to Ark 564 includes the Magellanic Stream extension (MSe), but this may also be LG (S03). As discussed above, if the UV- and X-ray–absorbing hot gas along the sight lines to F9 is the same, and if this gas is in CIE, the temperature in the MS is constrained to lie in the range $10^{5.75} < T < 10^{6.35}$ K. We detect little or no O VII or O VIII absorption toward Ark 564, which suggests that the temperature of the hot phase of the MSe is lower than that in the MS. Also in the southern Galactic hemisphere, the sight line to 3C 120 does not coincide with any large-scale local structure. Hot, local absorption along this sight line may correspond to the local WHIGM. In the northern Galactic hemisphere, the sight lines to NGC 3783, NGC 4593, and NGC 4051 overlap with the EPn structure as described by S03; however, we cannot obtain any temperature constraints along these sight lines, since these sources were not part of the S03 study. The sight line to NGC 5548 is not associated with any known local structure. Among the AGNs not contained in our sample but indicated in Figure 2, we note that the sight line to PKS 2155−304 (Nicastro et al. 2002; Fang et al. 2003) passes through the two HVCs that also lie along the sight lines to Mrk 509. The sight line to H1821+643 (Mathur et al. 2003) passes through the outer spiral arm, and the sight lines to both 3C 273 (Fang et al. 2003) and Mrk 421 (Cagnoni 2002; Rasmussen et al. 2003) passes through EPn. Of course there are Galactic sources that could contribute highly ionized oxygen along the sight lines to several of the AGNs. The Local Bubble can contribute at most only $\log N_{\rm O\ VII} \leq 15.48$, and radio loops, possibly corresponding to supernova remnants (SNR), along the sight line to 3C 273 could contribute $\log N_{\rm O\ VIII} \leq 15.90$ (Fang et al. 2003). The magnitudes of $N_{\rm O\ VII}$ and $N_{\rm O\ VIII}$ in Table 2 suggest that sources within the Milky Way contribute at most a small fraction of the O VII and O VIII column density along the sight lines to the AGNs in our sample.

6. IS APPARENT AGN OUTFLOW ACTUALLY DUE TO LOCAL ABSORPTION?

X-ray absorption that is apparently intrinsic to an AGN may actually be due to absorption by hot, local gas. For example, a low-velocity warm absorber component has been detected in NGC 4051 at a blueshift with respect to the AGN rest frame of -575 ± 175 km $\rm s^{-1}$ (Collinge et al. 2001) or -645 ± 130 km $\rm s^{-1}$ (McKernan et al. 2004). Since NGC 4051 is at $cz = 726 \pm 15$ km $\rm s^{-1}$, the apparent outflow from this source is equivalent to absorption at a redshift of $cz = +150 \pm 175$ km $\rm s^{-1}$ (using the Collinge et al. 2001 estimate) or $cz = +75 \pm 130$ km $\rm s^{-1}$ (using the McKernan et al. 2004 estimate) with respect to $z = 0$. This is certainly consistent with an origin in hot, local gas.

The spectra of QSOs with $cz >$ few thousand km $\rm s^{-1}$ highlight the ambiguity. For example, Pounds et al. (2003) detect an ionized outflow of $\sim$24,000 km $\rm s^{-1}$ in the *XMM-Newton* spectrum of PG 1211+143 with respect to the QSO rest frame. However, this quasar lies at $cz = 24{,}253 \pm 150$ km $\rm s^{-1}$, which suggests to us that a more likely explanation is absorption by hot, local gas (probably associated with Complex C). Similarly, Reeves et al. (2003) find that the *XMM-Newton* spectrum of PDS 456 requires a warm absorber with a very high outflow velocity ($47^{+35}_{-9} \times 10^3$ km $\rm s^{-1}$ from the EPIC pn instrument and $57^{+8}_{-10} \times 10^3$ km $\rm s^{-1}$ from the RGS instrument). However, the redshift of PDS 456 corresponds to a velocity offset of $cz = 55{,}200 \pm 300$ km $\rm s^{-1}$. Therefore, the warm absorption apparently intrinsic to PDS 456 could also be due to hot, local gas (probably associated with the Galactic center).

Figure 3 shows the offset velocity of absorption features relative to systemic AGN velocity versus cosmological recession

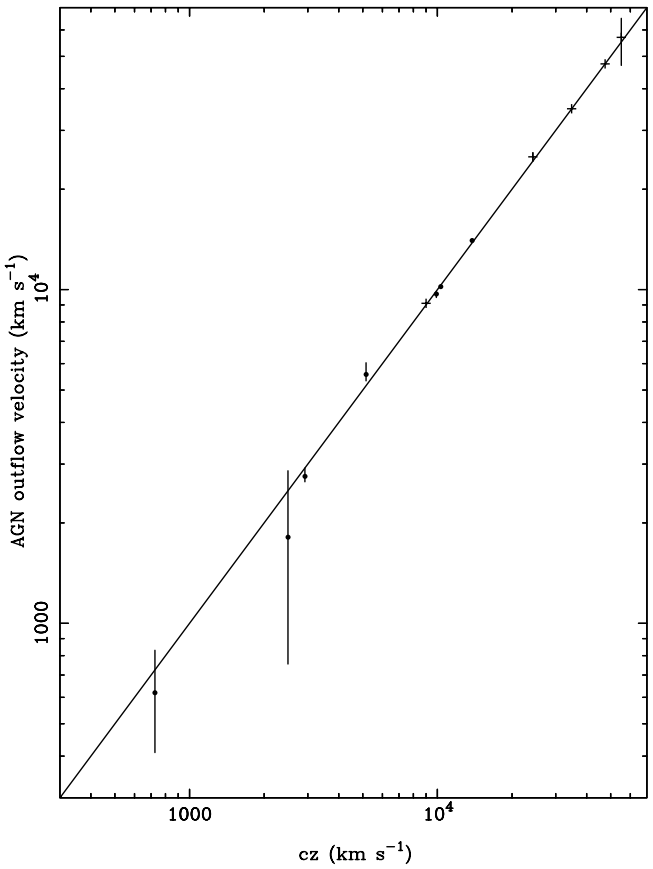

FIG. 3.—Plot of offset velocity of rest frame relative to AGN vs. cosmological recession velocity (cz) of AGN. *Filled circles*: AGNs from Table 2. *Plus signs*: AGN observations in the literature, including Mrk 421 (Cagnoni 2002; Rasmussen et al. 2003), PKS 2155−304 (Nicastro et al. 2002), 3C 273 (Fang et al. 2003), PDS 456 (Reeves et al. 2003), and PG 1211+143 (Pounds et al. 2003). The straight line corresponds to the LSR. Most of the errors on the velocity measurements are very small (few hundred km s^{-1}) relative to the actual offset velocity (few $\times 10^{3-4}$ km s^{-1}). The apparent AGN outflow detected in PDS 456 (*rightmost point*) by Reeves et al. (2003) and in PG 1211+143 (*fourth point from right*) by Pounds et al. (2003) seem to be better described by absorption at $z = 0$ since it seems unlikely that the AGN outflow velocity should be so similar to the redshifted velocity (cz) of the AGNs.

velocity (cz) of the AGNs. Filled circles denote AGNs listed in Table 2 and plus signs denote AGNs discussed in the literature. Clearly the absorption detected in PDS 456 (*rightmost point*) by Reeves et al. (2003) and in PG 1211+143 (*fourth point from right*) by Pounds et al. (2003) appear to be better described by absorption at $z = 0$, since it seems unlikely that the outflow velocity from the AGNs should be so similar to the recessional velocity (cz) of the AGNs. The correlation in Figure 3 is impressive, which suggests that apparent outflows in other AGNs may also be due to absorption by hot, local gas.

Pounds et al. (2003) and Reeves et al. (2003) detected absorption signatures both in the Fe K band, around 6.4 keV, and at lower energies in the *XMM-Newton* spectra of the QSOs PG 1211+143 and PDS 456, respectively. They use the apparent kinematic agreement between the low-energy and Fe K band signatures as well as the high ionic column density required by the Fe K band signatures to conclude that the absorption is intrinsic to the AGN. However, it is clear from the present work (in particular Fig. 3) that low energy absorption signatures due to hot, local gas are relatively common and should therefore be expected in QSO spectra. Therefore, a kinematic agreement between low energy absorption signatures and Fe K band absorption signatures does not ipso facto support an intrinsic AGN origin. Furthermore, the large ionic column density derived from the Fe K band absorption signatures in both cases comes from photoionization modelling, the use of which is unwarranted if the absorber is local, hot gas. We also note that the spectral resolution of the *XMM-Newton* CCDs in the Fe K band is at least an order of magnitude worse than that of the gratings at the energies of O VII (r) and O VIII Lyα. Absorption features in the Fe K band may be a blend of multiple features, which may or may not be individually resolved by CCDs, and this can impact interpretation of the data. Indeed a blend of unresolved absorption features in the Fe K band could account for the very large ionic Fe column inferred from photoionization modelling that led Pounds et al. (2003) and Reeves et al. (2003) to reject a local origin for the absorption. We therefore conclude that the assumption that the absorption is intrinsic to the quasar, which in turn leads to the conclusion of a relativistic outflow, is not supported by our analysis and results.

7. CONCLUSIONS

We have assembled a small sample of type I AGNs observed with the high resolution X-ray gratings on board *Chandra* and have applied a uniform analysis to detect soft X-ray absorption by hot gas in the vicinity of our Galaxy. Around half of the sight lines in our sample exhibit local ($z = 0$) O VII (r) or O VIII absorption (or both) at $\geq$90% confidence. We identify the absorption features with hot gas in local structures, following the discussion in S03 of local O VI absorption. Several sight lines in our sample coincide with sight lines in the S03 study, and so it is possible to derive constraints on the temperature of the local hot gas, assuming collisional ionization equilibrium (CIE).

In the northern Galactic hemisphere, we detect strong absorption by local O VII (r) along the sight lines to NGC 3783 and NGC 4051 (which also exhibits O VIII absorption). These sight lines (and that toward NGC 4593) overlap with the EPn local structure discussed by S03. The sight line toward NGC 5548 shows local O VII and O VIII absorption, implying that the gas temperature is $T > 10^{6.2}$ K if the gas is in CIE, and we use the S03 upper limit on $N_{\rm O\ VI}$ along this sight line. In the southern Galactic hemisphere, we can identify absorption along the sight line to F9 with the Magellanic Stream (MS). O VI is detected toward F9 by S03, and if we associate our detection of O VII absorption with the same gas, then $10^{5.75} < T < 10^{6.35}$ K if the gas is in CIE. There is a hint of broad O VII absorption along the sight line toward Mrk 509. S03 and Collins et al. (2004) suggest that Local Group clouds along this sight line interact with a hot Galactic corona or a low density LG medium (the $z = 0$ WHIGM); if so, CIE is unlikely. The sight line to 3C 120 does not appear to be associated either with local structure or UV-absorbing gas (S03), and so absorption may result from local WHIGM. The local gas along the sight line to Ark 564 has $T < 10^{6.10}$ K if it is in CIE. A very important point to note is that the apparent warm, high-velocity outflows detected in PG 1211+143 (Pounds et al. 2003) and PDS 456 (Reeves et al. 2003) could actually correspond to absorption by hot gas in the vicinity of our Galaxy. The low velocity warm absorber in NGC 4051 (Collinge et al. 2001; McKernan et al. 2004) could also correspond to local absorption. The correlation in Figure 3 is so strong that it seems likely that absorption by hot, local gas may account for apparent outflows in other AGNs.

This is the first attempt to systematically investigate the X-ray–absorbing hot gas in the vicinity of the Galaxy. We have detected multiple absorption signatures along several sight lines through this gas at confidence levels ranging from >90% to >3 σ. Some of the gas is associated with known local structures, and some may be associated with the local WHIGM. Obviously the size of our present sample is the main limitation on our investigation of the local, hot gas. We need many more sight lines through the local $z = 0$ hot gas to begin to constrain and genuinely map the WHIGM and the hot phase of local structures.

We gratefully acknowledge support from NSF grant AST 0205990 (B. M.) and NASA grants G01 2102X, G02 3133X, and AR4-5009X issued by CXC operated by SAO under NASA contract NAS8-39073 (T. Y.). Thanks to Smita Mathur for useful discussions. We made use of the HEASARC online data archive services, supported by NASA/GSFC, and also the NASA/IPAC Extragalactic Database (NED), operated by the Jet Propulsion Laboratory, California Institute of Technology, under contract with NASA. Thanks to the *Chandra* instrument and operations teams for making the observations possible.

REFERENCES

Cagnoni, I. 2002, preprint (astro-ph/0212070)
Cash, W. 1976, A&A, 52, 307
Cen, R., & Ostriker, J. P. 1999, ApJ, 514, 1
Collinge, M. J., et al. 2001, ApJ, 557, 2
Collins, J. A., Schull, J. M., & Giroux, M. L. 2004, ApJ, 605, 216
Davé, R., et al. 2001, ApJ, 552, 473
Elvis, M., Wilkes, B. J., & Lockman, F. J. 1989, AJ, 97, 777
Fang, T., Marshall, H. L., Lee, J. C., Davis, D. S., & Canizares, C. R. 2002, ApJ, 572, L127
Fang, T., Sembach, K. R., & Canizares, C. R. 2003, ApJ, 586, L49
George, I. M., Turner, T. J., Netzer, H., Nandra, K., Mushotzky, R. F., & Yaqoob, T. 1998, ApJS, 114, 73
Heckman, T. M., Norman, C. A., Strickland, D. K., & Sembach, K. R. 2002, ApJ, 577, 691
Hellsten, U., Gnedin, N. Y., & Miralde-Escudé, J. 1998, ApJ, 509, 56
Markert, T. H., Canizares, C. R., Dewey, D., McGuirk, M., Pak, C., & Shattenburg, M. L. 1994, Proc. SPIE, 2280, 168
Mathur, S., Weinberg, D. H., & Chen, X. 2003, ApJ, 582, 82
McKernan, B., Yaqoob, T., George, I. M., & Turner, T. J. 2003a, ApJ, 593, 142
McKernan, B., Yaqoob, T., Mushotzky, R., George, I. M., & Turner, T. J. 2003b, ApJ, 598, L83
McKernan, B., Yaqoob, T., & Reynolds, C. S. 2004, MNRAS, submitted
Murphy, E. M., Lockman, F. J., Laor, A., & Elvis, M. 1996, ApJS, 105, 369
Nicastro, F., et al. 2002, ApJ, 573, 157
Perna, R., & Loeb, A. 1998, ApJ, 503, L135
Pounds, K. A., Reeves, J. N., King, A. R., Page, K. L., O'Brien, P. T., & Turner, M. J. L. 2003, MNRAS, 345, 705
Rasmussen, A., Kahn, S. M., & Paerels, F. 2003, in ASSL Conf. Proc. 281, The IGM/Galaxy Connection: The Distribution of Baryons at $z = 0$, ed. J. L. Rosenberg & M. E. Putman (Dordrecht: Kluwer), 109
Reeves, J. N., O'Brien, P. T., & Ward, M. J. 2003, ApJ, 593, L65
Reynolds, C. S. 1997, MNRAS, 286, 513
Sembach, K. R., Savage, B. D., Lu, L., & Murphy, E. M. 1999, ApJ, 515, 108
Sembach, K. R., et al. 2003, ApJS, 146, 165 (S03)
Stark, A. A., Gammi, C. F., Wilson, R. W., Bally, J., Linke, R. A., Hiles, C., & Hurwitz, M. 1992, ApJS, 79, 77
Sutherland, R. S., & Dopita, M. A. 1993, ApJS, 88, 253
Tripp, T. M., Savage, B. D., & Jenkins, E. B. 2000, ApJ, 534, L1
Verner, D. A., Ferland, G. J., Korista, K. T., & Yakovlev, D. G. 1996, ApJ, 465, 487

Note added in proof.—If we associate the high iron column density along the sight lines to PG 1211+143 and PDS 456 with hot local gas, a significant change in our understanding of the Galactic environment is required.